Ab initio structural and electronic properties of dangling-bond-free SiO$_x$N$_y$

Alberto Martinez-Limia, Philipp Plänitz, and Christian Radehaus

Institute for Electrical and Information Engineering, TU Chemnitz, 09112 Chemnitz, Germany

Using *ab initio* density-functional theory we investigate the influence of electrically inactive nitrogen defects in a silica matrix on the geometry and electronic structure of the material. The generation of these defects is discussed. Structure, total energy, and density of electronic states are reported for low concentrations. We find that for the studied concentrations the short range structure of the oxide is preserved while in the long range the material becomes increasingly amorphous with growing nitrogen content. The effect on the stabilization of oxygen defects and on oxygen diffusion is discussed. Reduction of the SiO$_2$ band gap and other changes in the density of states with increasing nitrogen concentration are observed and correlated with experimental data.

I. INTRODUCTION

Scaling down metal-oxide-semiconductor (MOS) devices implies the continuous reduction of the SiO$_2$ gate layer that so far is used as gate dielectric. However, scaling this layer below a certain thickness (2−3 nm) is problematic.[1] The first problem arises from the exponential increase of the charge carrier tunneling probability by decreasing thickness of the SiO$_2$ layer, resulting in an unacceptably large leakage current. Other problems are related to the reliability of the devices. During operation of the MOSFET carrier flow and dopant diffusion result in the generation of defects in addition to the original defects of the dielectric material and of the Si/SiO$_2$ interface. As the dielectric layer thickness decreases the critical density of defects that induces a breakdown of devices decreases as well.

Until the desired long term solution for these problems appears in the form of a reliable high-κ material, present technology relies on the incorporation of N into the SiO$_2$ layer for the improvement of the performance of the gate dielectric.[2,3] On one side the incorporation of N should enhance the dielectric constant of the SiO$_2$ making thicker dielectric layers with corresponding low tunneling probability and lower leakage current possible. On the other side the incorporated N atoms generate a better barrier to dopant and oxygen diffusion in the oxide. These properties combined with the increased physical thickness of the dielectric layer should enhance the reliability.

There is no complete picture about the bonding configurations of N atoms incorporated into SiO$_2$. Physical properties of SiO$_x$N$_y$ films depend on the composition and deposition technique, which influence the local structure.[4] Some theoretical calculations point at the generation of dangling bonds, lone pairs of the involved atoms (N, Si, O), and over-coordinated oxygen atoms[2] in these compounds compared to pure SiO$_2$. Recent calculations show the possibility to create an electrically inactive, very stable complex of a pair of threefold coordinated N atoms in a crystalline α-quartz matrix.[5,6] The formation of this complex [N(3)$_O$-V_O-N(3)$_O$] would annihilate O vacancies and complete the coordination of N atoms reducing the number of dangling bonds in material. This type of complex seems to be the dominant inactive N defect in amorphous silicon oxynitride.[5,6]

Previous work has been done to calculate the electronic structure of silicon dioxide with *ab initio* methods.[7–10] The known crystalline phases of the SiO$_x$N$_y$ system have been modeled using the density-functional theory (DFT) and the local-density approximation.[11,12] So far *ab initio* calculations of amorphous silicon oxynitride containing defects in the form of under-coordinated nitrogen atoms with concentrations around 10% have been performed.[13] For the modeling of systems with lower concentrations of nitrogen, which are particularly interesting for MOS applications, big unit cells with more than one hundred atoms are required.

In this paper the influence of nitridation at low N concentrations (below 10 percent) on the structural and electronic properties of SiO$_2$ is theoretically investigated. We focus on dangling bond free structures obtained by the introduction of the N(3)$_O$-V_O-N(3)$_O$ complex into α quartz. A detailed discussion of other N related defects was published elsewhere.[5,6] Dangling bond free materials with no extra levels in the band gap are particularly interesting for technological applications, and studying them as model systems provides the necessary insight to improve fabrication processes.

Using DFT we first investigate the reaction mechanism that leads to the formation of N(3)$_O$-V_O-N(3)$_O$ on α quartz starting from isolated twofold coordinated N atoms and O vacancies. We investigate structural properties of nitridated SiO$_2$ obtained by addition of N(3)$_O$-V_O-N(3)$_O$ at different low concentrations calculating minimal energy configurations and pair and angle distributions. The transition from crystalline to amorphous phase is described as well as local changes around the nitrogen atoms and their implications for the diffusion of other atomic or molecular species. In addition the electronic properties of the materials, including band gap and density of states (DOS), are calculated and correlated with the nitrogen content on these systems.

II. COMPUTATIONAL METHODS

The calculations have been done with DFT in the local-density approximation (LDA) using a plane wave basis set with an energy-cutoff of 60 Rydberg and periodic boundary conditions. Pseudopotentials of Troullier-Martins type[14] gen-
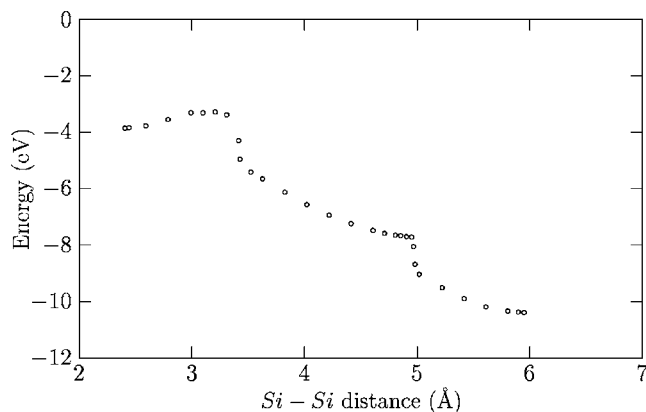
FIG. 1. Energy variation along the dissociation path.

erated by Khein and Allanwere[15] were used. The CPMD code[16] was used for the calculations described in Secs. III and IV A.

The formation of the $N(3)_O$-V_O-$N(3)_O$ defect was investigated starting with an α quartz supercell with 36 Si atoms, generated by repeating the hexagonal ground cell (space group $P3_221$, $a=b=4.913$ Å, $c=5.405$ Å, 9 atoms)[17] 3, 2, and 2 times in x, y, and z directions, respectively. Two N atoms were included in the supercell substituting two O atoms and opposite sites of a created O vacancy [$2N(2)_O$ $+V_O$ configuration]. Several structures along the investigated reaction path were fully relaxed for fixed lengths of the reaction coordinate. These relaxations were done for the Gamma-point until the remaining force on each atom was less than 5 mRy/Å. For other details see Sec. III.

The generation of the amorphous SiO_xN_y structures described in Sec. IV A consisted of a three steps procedure. First, the defects were included in a perfect α quartz supercell (with similar structure as in the previous case) for the desired concentrations. Second, using Car-Parrinello molecular dynamics simulated annealing for a total time of 0.6 ps with starting temperature of 1200 K, exponential temperature decay and final temperature under 50 K was done. A fictitious electronic mass of 600 a.u. was employed to achieve a stable molecular dynamics run. Finally, the structures obtained by the annealing were fully relaxed until the atomic forces were under the 5 mRy/Å threshold. For other details see Sec. IV A.

The ABINIT code[15,18–20] was used to calculate the electronic properties presented in Sec. IV B for crystalline and amorphous structures. Reported unit cell parameters for the crystalline phases of α quartz (α-SiO_2), Si_2N_2O and β-Si_3N_4 have slight variations in the literature. In this work we used for α-SiO_2 the hexagonal ground cell, space group $P3_221$, $a=b=4.913$ Å, $c=5.405$ Å, 9 atoms;[17] for Si_2N_2O the orthorhombic ground cell, space group $Cmc2_1$, $a=8.843$ Å, $b=5.437$ Å, $c=4.835$ Å, 20 atoms;[21] and for β-Si_3N_4 the hexagonal ground cell, space group $P6_3m$, $a=b=7.606$ Å, $c=2.909$ Å, 14 atoms.[22] Additionally, the amorphous SiO_xN_y structures generated with CPMD were used. For the calculation of electronic properties, after checking for convergence with respect to the density of k points in the reciprocal space, a Monkhorst-Pack[23] k-point set of $4\times4\times4$ for the SiO_xN_y structures and $6\times6\times6$ for the crystalline phases was used for the integration over the Brillouin zone.

III. THE FORMATION OF $N(3)_O$-V_O-$N(3)_O$ DEFECTS

Since twofold coordinated N atoms can occupy the place of O atoms in the silicon dioxide network [$N(2)_O$], it is expected that the nitridation of quartz starts by forming this sort of configurations on O-poor conditions. In the presence of additional O vacancies (V_O) the reaction $2N(2)_O+V_O$ forming $N(3)_O$-V_O-$N(3)_O$ could occur. Lee and Chang determined this reaction to be exothermic by 6.2 eV.[5] Since the reaction involves Si-Si bond breaking and movement of Si atoms over considerable distance we have investigated the reaction path to establish the necessary activation energy of the process.

The reaction path starts from a $2N(2)_O$-V_O configuration, going over a $N(3)_O$-$N(2)_O$-V_O, to the final $N(3)_O$-V_O-$N(3)_O$ configuration. The reaction coordinate is the distance between the Si atoms that form the dimer in the start configuration. These two atoms move apart from each other breaking the Si-Si bond and bonding to the $N(2)_O$ atoms for the completion of their coordination. The reaction is exothermic by 6.52 eV (which is close to the result of Lee and Chang[5]) and requires an activation energy of 0.54 eV (see Figs. 1 and 2).

The reaction path goes uphill between 2.40 and 2.99 Å corresponding to the breaking of the Si-Si bond; a plateau

2.401Å
-3.86eV

3.208Å
-3.29eV

4.650Å
-7.48eV

4.954Å
-7.72eV

5.951Å
-10.39eV
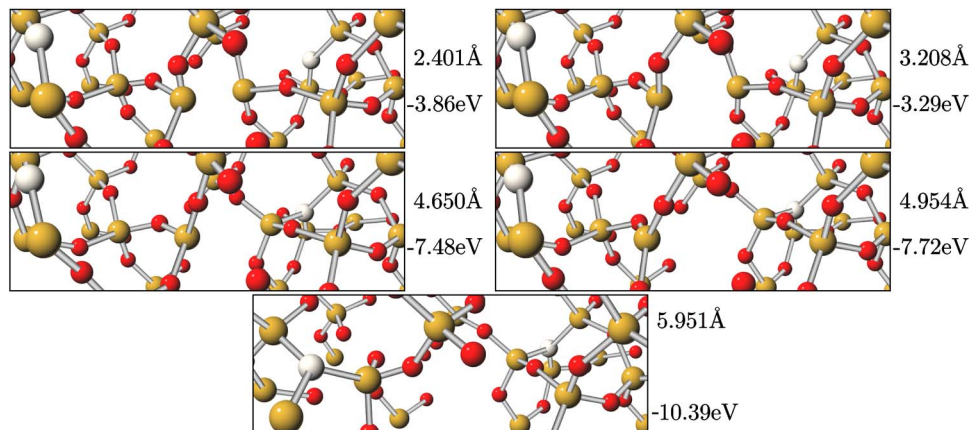
FIG. 2. (Color online) Atomic structures along the Si-Si dissociation and $N(3)_O$-V_O-$N(3)_O$ formation. [Gray (yellow online): Si, dark gray (red online): O, white: N].

TABLE I. Concentrations of Si, N, and O for the known and the calculated structures of SiO_xN_y.

Structure	x	y	ξ (%)	Si (%)	O (%)	N (%)
SiO_2	2.0	0.0	0.0	33.33	66.67	0.00
$N_{2\%}$	1.92	0.06	2.82	33.64	64.49	1.87
$N_{4\%}$	1.83	0.11	5.71	33.96	62.26	3.77
$N_{6\%}$	1.75	0.17	8.70	34.29	60.00	5.71
$N_{8\%}$	1.67	0.22	11.76	34.62	57.69	7.69

follows between 2.99 and 3.30 Å where the first Si atom moves across the plane of the three O atoms bound to it. The reaction continues downhill while the new N-Si bond forms slowing down on a new plateau (4.72–4.95 Å) where the second Si atom shifts in a similar way as the first one did across the O plane to finally bound to the second N atom when the distance Si-Si is about 5.95 Å. This reaction is very likely to take place under the condition that the two original $N(2)_O$ are in the favorable position, between 4 and 6 Å away of an O vacancy and at opposite sides of it. The resulting configuration is very stable and the positions of the two $N(3)_O$ atoms are strongly correlated.

For a better nitridation, N atoms should be added in a process occurring in an O deficient environment to increase the possibility of finding appropriate places around O vacancies that favor the formation of $N(3)_O$.[5,6] This explains the more probable location of N atoms near to the Si/SiO_2 interface where the O concentration is lower.[24] Moreover, $N(2)_O$-type defects are also more stable in the absence of competing O.

IV. NITRIDATED SiO2

A. Structural properties

To study the structural and electronic properties of nitridated SiO_2 we propose a series of structures for SiO_xN_y with a rather big periodic supercell for different values of x and y (see Table I). Previous theoretical simulations shows that for low concentration of N ($\xi = \frac{y}{x+y} < 13\%$) the structure of the oxide matrix is preserved,[13] while experimental infrared absorption spectra reveal a structure very close to SiO_2 for the used concentrations.[25] As shown in the previous section the $N(3)_O$-V_O-$N(3)_O$ are extended structures in the α-quartz matrix and they can be included only in a limited number of physical places for a given supercell size. Higher N concentrations without dangling bonds could be achieved by changing drastically the original structure. In this case we expect structures with extended Si-N planes like in crystalline Si_2N_2O.

We started with an α-quartz crystal structure containing 36 Si atoms and substituted 3, 6, 9, and 12 O atoms by 2, 4, 6, and 8 N atoms respectively. The new structures are formed by $N(3)_O$-V_O-$N(3)_O$ pairs. The $N(3)_O$-V_O-$N(3)_O$, pairs were distributed uniformly in the unit cell. The supercells have no dangling bonds and are constructed in accordance to the tetrahedron model and Motts rule[26] for amorphous SiO_xN_y.
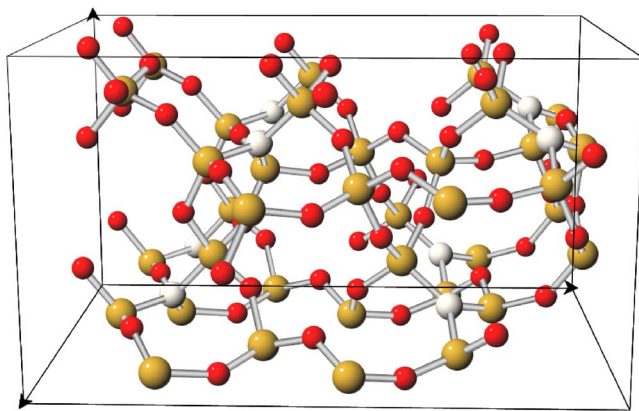
FIG. 3. (Color online) Optimized structure for $SiO_{1.67}N_{0.22}$ [gray (yellow online): Si, dark gray (red online): O, white: N].

Other N related defects are not included because it was established that they include dangling bonds and/or are energetically unfavorable. Isolated $N(3)_O$ could exist in amorphous material but cannot be added in a similar form in α quartz without dangling bonds.

The structures were annealed following the procedure described in Sec. II. Even for the high temperature phase of the simulated annealing ($T \geqslant 1000$ K) no bond breaking was observed in the material. Only small shifts and oscillations around the original positions were observed, indicating a high thermal stability of the material. After annealing the structures were optimized until the forces on all atoms were below the given threshold. The final structure for $N_{8\%}$ is shown in Fig. 3. Similar structures were obtained for $N_{2\%}$, $N_{4\%}$, and $N_{6\%}$.

The results for the total energy depending on the N concentration are shown in Table III. The total energy changes linear with increasing N concentration which gives evidence of the homogeneous distribution of the $N(3)_O$-V_O-$N(3)_O$ pairs, and of the weak interaction between them.

The partial pair-distribution functions $g_{A\text{-}B}(r)$ between the atomic species A and B of the modeled systems for 4 and 8% N compared to the α quartz are shown in Fig. 4. The first peaks for the $g_{N\text{-}Si}(r)$ and $g_{O\text{-}Si}(r)$ at 1.72 and 1.61 Å, respectively, are very sharp for all systems and show the short range order of the structure with tetrahedral Si-centered basic units. The observed broadening of the first Si-Si and O-O peaks with respect to the same sharp peaks in α quartz points to an increasingly amorphous character of the structure with increasing N content. Particularly the peaks on the $g_{Si\text{-}Si}(r)$ of α quartz at 4.36 and 4.90 Å practically disappear in the nitridated material, even for the 4% system. These peaks represent the distance between the Si atoms centered on tetrahedral units separated by one or two other units and give the geometrical dimensions of the interstitials on α quartz. Simple inspection of the structure of Fig. 3 shows that the N atoms occupy these interstitials anchoring Si atoms from opposite sides of it and reducing the flexibility of the structure. Since the diffusion of molecular O_2 [the preferred chemical form of diffusing O in SiO_2 (Ref. 27)] is highly dependent on the connectivity of the interstitial network in the oxide,[28,29] reducing the connectivity has a nearly exponential influence
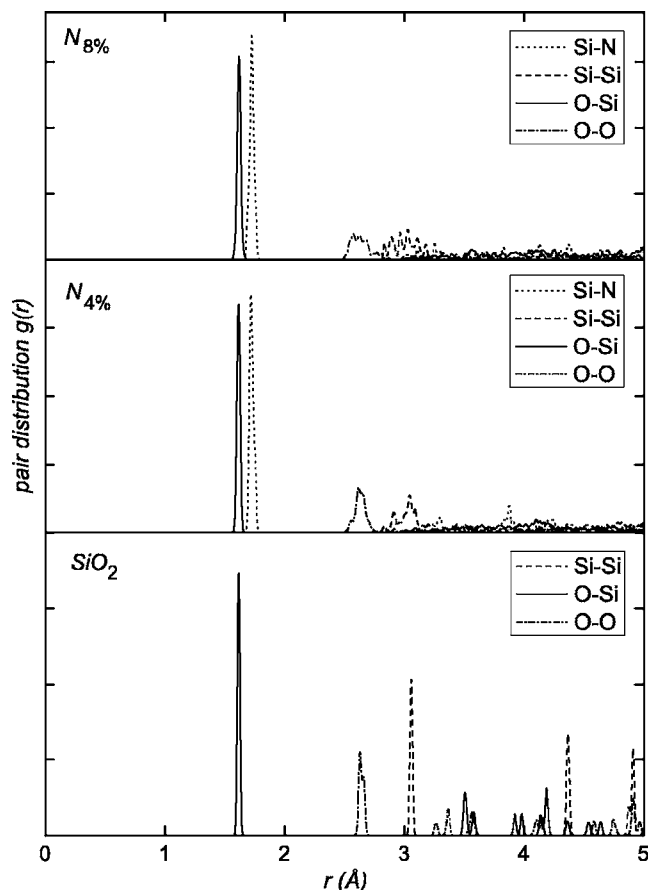
FIG. 4. Pair distribution for SiO_2 and SiO_xN_y.

FIG. 5. Angle distribution for SiO_2 and SiO_xN_y.

on the increase of the activation energy necessary for O_2 to diffuse. A similar influence on the diffusion of other dopants is expected.

The angle-distribution functions between the atoms of the modeled systems are shown in Fig. 5 compared to similar distribution functions for α quartz. While for all the angles we observe some broadening with respect to the values in the ideal crystal this effect is particularly important for the Si-O-Si angle distribution. These are the angles that are most affected by the increasingly amorphous character of the original crystal structure since they determine the relative position of the tetrahedrons centered on the Si atoms that form the ground structural units.

B. Electronic properties

The results of our electronic structure calculations for crystalline α-SiO_2, Si_2N_2O, and β-Si_3N_4 are presented in Table II compared to reference calculations and experimental values in the literature.

As expected the band gap turns smaller with increasing nitrogen content in the crystalline phases. The values are in good agreement with LDA results from other groups. The LDA is known to underestimate the band gap of semiconductors up to 50%. The bands can be corrected to a good approximation by a shift of the conduction bands, to fit the experimental value of the band gap. A comparison of the

LDA and the experimental values of Table II shows that different shifts are needed to correct the results of the different systems. However, given the small concentration of nitrogen in our SiO_xN_y we assume a constant shift (the same shift as for α-SiO_2) of the calculated band gaps with respect to the exact value, so that the results for our different amorphous systems are comparable.

Calculations of the electronic properties (total energy and DOS) for the SiO_xN_y structures (see Table I) have been done. The results for the electronic structure are given in Table III. The total energy per valence electron changes linearly with increasing nitrogen concentration. The values for the SiO_xN_y structures fit to the values for the crystalline α-SiO_2 and Si_2N_2O phases.

TABLE II. Calculated electronic properties of different crystalline phases of the SiO_xN_y system.

	α-SiO_2	Si_2N_2O	β-Si_3N_4
Total energy (Ha)	−113.4	−186.3	−110.7
Energy per valence electron (Ha)	−2.36	−1.94	−1.73
Band gap (eV)	5.88	5.12	4.22
Reference calculation for band gap (eV)	5.59 (Ref. 7)	5.20 (Ref. 11)	4.96 (Ref. 11)
Experimental band gap (eV)	8.9 (Ref. 1)	5.7 (Ref. 33)	5.1 (Ref. 1)

TABLE III. Calculated electronic properties for amorphous phases of the SiO_xN_y system.

N in %	1.87	3.77	5.71	7.69
Total energy E_{tot} in Ha	−1331.2	−1302.1	−1273.1	−1237.6
Energy per valence electron (Ha)	−2.34	−2.325	−2.306	−2.275
Band gap E_{gap} in eV	5.19	5.16	5.05	4.79

A plot of the calculated density of states (DOS) is shown in Fig. 6. If we compare the DOS for SiO_xN_y with those of pure SiO_2 we see new states inside the original band gap of α quartz which have a slightly higher energy level as the top of the original valence band. This effect intensifies with increasing nitrogen content. This is in agreement with photoemission spectroscopy measurements by Toyoda.[30] The bottom of the conduction band remains practically unchanged. This fact supports our assumption of a constant shift of the calculated conduction band for our SiO_xN_y systems and the crystalline SiO_2 with respect to experimental values. The absence of new states in the middle of the gap confirms the electrically inactive character of the $N(3)_O$-V_O-$N(3)_O$ defects. The energy level for the N 2s states is about −14 eV, the corresponding peak in the DOS becomes broadened and higher for increasing nitrogen content.
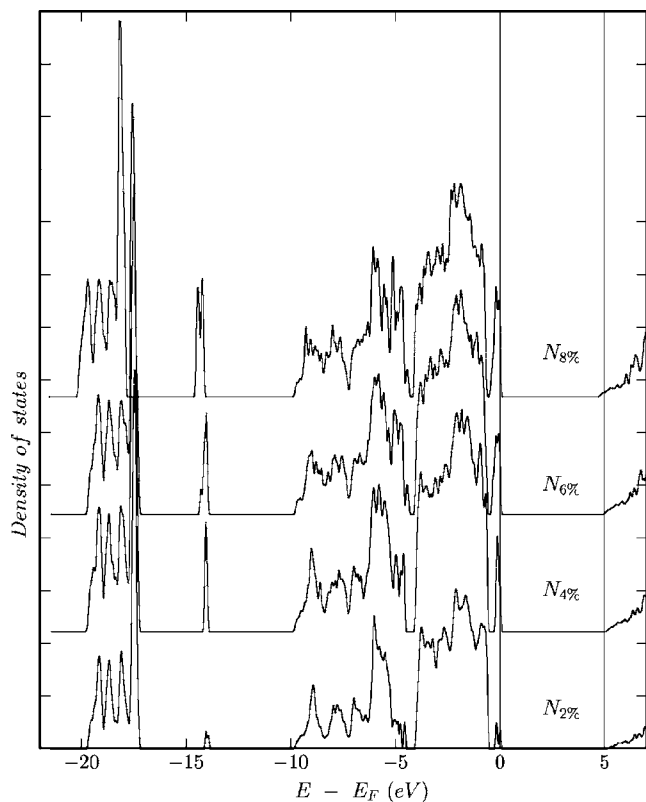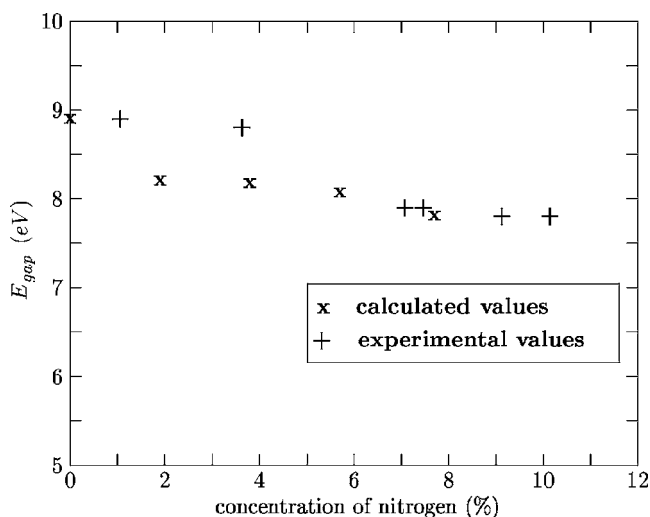
FIG. 7. Band gaps for the SiO_xN_y system.

In Fig. 7 the values of the shifted band gaps for the crystalline SiO_2 and the SiO_xN_y systems are shown. The shift of 3.02 eV is taken to fit the experimental value of 8.9 eV for SiO_2. Experimental values are also plotted in the diagram.[32] Our results show that the inclusion of N is responsible for a reduction of the band gap by 0.5 eV already for the lowest concentration. It is plausible that the experiment, in contrast to the theory, could not measure this effect. The increasingly amorphous character of the structures that appears when going from $N_{2\%}$ to $N_{8\%}$ is responsible for a reduction of the band gap by additional 0.5 eV. A similar effect was observed for crystalline α quartz and amorphous silica by previous XPS measurements.[31] The band gap shows a nonlinear dependency on the nitrogen concentration for the SiO_xN_y structures.

V. CONCLUSIONS

The present work described the inclusion of N atoms in α quartz for concentrations up to 8% and the physical and electronic properties of the material. In contrast to results from other authors in similar studies,[13] the proposed material has no defects in form of under-coordinated atoms and no extra inclusion of hydrogen atoms is necessary for passivation and the corresponding partial recovering of the band gap of α quartz.[13] The presence of H atoms in gate oxides is undesirable due to reliability considerations;[34] hence the simulated materials are especially attractive for this kind of application. The defects in the $N(3)_O$-V_O-$N(3)_O$ configuration are very stable and could not be included in higher concentrations in the original α-quartz structure. For higher N concentrations we expect a phase change with extended Si-N planes as in crystalline Si_2N_2O. These structural characteristics have a direct impact in the (oxy-)nitridation technology needed for the fabrication of a material with a desired N concentration.

The primary effects of N inclusion are neutralization of O vacancies, deposition near to SiO_2/Si interface, increasingly amorphous character of the structure, reduction of the flexibility of the structure and reduction of connectivity of the interstitial network. This has a direct influence on the reduc-

FIG. 6. Density of states for four different unit cells of SiO_xN_y (from bottom to top: $N_{2\%}$, $N_{4\%}$, $N_{6\%}$, and $N_{8\%}$). The Fermi level is placed over the last occupied energy level. The presented data are the result of a convolution with a Gaussian of width $\sigma = 50$ meV.

tion of diffusion of other species in the material, a desirable property for microelectronic applications.

Analyzing the DOS, and comparing it with experimental results, we identified two contributions to the narrowing of the band gap. First, new states arise near the top of the original valence band of SiO_2. These states become broader with increasing N concentration. Second, the increasingly amorphous character of the system contributes to additional narrowing of the band gap. In the structures investigated all the Si atoms are fourfold coordinated which prevents the arising of additional states in the gap reported by other authors.[13] This is favorable for applications of the investigated material as gate dielectric.

[1] M. Houssa, *High-k Gate Dielectrics* (Institute of Physics Publishing, London, 2004).

[2] S. Jeong and A. Oshiyama, Phys. Rev. Lett. **86**, 3574 (2001).

[3] N. Y. K. Muraoka, K. Kurihara, and H. Satake, J. Appl. Phys. **94**, 2038 (2003).

[4] W. L. Scopel, A. J. R. daSilva, W. Orellana, R. J. Prado, M. C. A. Fantini, A. Fazzio, and I. Pereyra, Phys. Rev. B **68**, 155332 (2003).

[5] E.-C. Lee and K. J. Chang, Phys. Rev. B **66**, 233205 (2002).

[6] E.-C. Lee and K. J. Chang, Physica B **340-342**, 974 (2003).

[7] Y. N. Xu and W. Y. Ching, Phys. Rev. B **44**, 11048 (1991).

[8] J. Sarnthein, A. Pasquarello, and R. Car, Phys. Rev. Lett. **74**, 4682 (1995).

[9] J. Sarnthein, A. Pasquarello, and R. Car, Phys. Rev. B **52**, 12690 (1995).

[10] J. H. Th. Demuth, Y. Jeanvoine, and J. Angyan, J. Phys.: Condens. Matter **11**, 3833 (1999).

[11] Y. N. Xu and W. Y. Ching, Phys. Rev. B **51**, 17379 (1995).

[12] A. Y. Liu and M. L. Cohen, Phys. Rev. B **41**, 10727 (1990).

[13] D. Fischer, A. Curioni, S. Billeter, and W. Andreoni, Phys. Rev. Lett. **92**, 236405 (2004).

[14] N. Troullier and J. L. Martins, Phys. Rev. B **43**, 1993 (1991).

[15] The ABINIT code is a common project of the Universite Catholique de Louvain, Corning Incorporated, and other contributors (URL: http://www.abinit.org)

[16] CPMD code, copyright IBM Corp. 1990–2004, copyright MPI für Festkörperforschung Stuttgart (1997–2001).

[17] R. W. G. Wyckoff, *Crystal Structures* (Interscience Publishers, New York, 1964).

[18] X. Gonze, J.-M. Beuken, R. Caracas, F. Detraux, M. Fuchs, G.-M. Rignaese, L. Sindic, M. Verstraete, G. Zerah, and F. Jollet, Comput. Mater. Sci. **25**, 478 (2002).

[19] X. Gonze, Phys. Rev. B **54**, 4383 (1996).

[20] M. Payne, M. Teter, D. Allan, D. Arias, and J. Joannopoulos, Rev. Mod. Phys. **64**, 1045 (1992).

[21] C. Brosset and I. Idrestedt, Nature (London) **201**, 1211 (1964).

[22] L. Cartz and J. D. Jorgensen, J. Appl. Phys. **52**, 236 (1981).

[23] H. J. Monkhorst and J. D. Pack, Phys. Rev. B **13**, 5188 (1976).

[24] E. P. Gusev, H.-C. Lu, and M. L. Green, IBM J. Res. Dev. **43**, 265 (1999).

[25] A. del Prado, E. San Andres, I. Martil, G. Gonzalez-Diaz, D. Bravo, F. J. Lopez, M. Fernandez, and F. L. Martinez, J. Appl. Phys. **94**, 1019 (2003).

[26] N. F. Mott, Adv. Phys. **16**, 49 (1967).

[27] W. Orellana, A. J. R. da Silva, and A. Fazzio, Phys. Rev. Lett. **87**, 155901 (2001).

[28] A. Bongiorno and A. Pasquarello, Phys. Rev. Lett. **88**, 125901 (2002).

[29] A. Bongiorno and A. Pasquarello, Phys. Rev. B1 **70**, 195312 (2004).

[30] K. O. S. Toyoda, J. Okabayashi, H. Kumigashira, M. Oshima, K. Ono, M. Nima, K. Usuda, and N. Hirashita, Appl. Phys. Lett. **83**, 5449 (2003).

[31] T. Stephenson and N. J. Binkowski, J. Non-Cryst. Solids **22**, 399 (1976).

[32] C. Ance, F. de Chelle, J. P. Ferraton, and G. Leveque, Appl. Phys. Lett. **60**, 1399 (1992).

[33] V. A. Gritsenko, N. D. Dikovskaja, and K. P. Magilnikoo, Thin Solid Films **51**, 353 (1978).

[34] J. H. Stathis, IBM J. Res. Dev. **46**, 265 (2002).